Soft Matter

Cite this: *Soft Matter*, 2012, **8**, 5835

www.rsc.org/softmatter

**PAPER**

# Hydrophobic counter ion effects on the formation of mesh and reversed phases in the perfluorodecanoate/water system

**Rongrong Zhou,[a] Michael Holmes,*[b] Smita Puntambekar,[c] Marc Leaver[d] and Richard McCabe[a]**

***Received 9th February 2012, Accepted 28th March 2012***
**DOI: 10.1039/c2sm25295c**



The tetramethylammonium perfluorodecanoate ($C_{10}$TMA)/water system forms both random, $Mh_1(0)$ and correlated mesh, $Mh_1(R\bar{3}m)$ phases over a wide range of concentration and temperature. Whilst the random mesh phase is found in the ammonium homologue, the extensive correlated mesh phase seems to be a result of the hydrophobic nature of the tetramethylammonium (TMA) counter ion. In order to explore the reasons for the occurrence of these mesh phases and the effects of hydrophobic counter ions on phase structure the counter ion has been substituted by a series of increasing hydrophobicity namely butyltrimethylammonium (BTMA), dibutyldimethylammonium (DBDMA), and methyltributylphosphonium (MTBP). The phases and their structures were identified by small angle X-ray scattering. Increasing counter ion hydrophobicity causes a change from mesh, to lamellar, and finally to reversed phases. All the hydrophobic counter ions are strongly bound to the water/fluorocarbon interface and, in the case of those with butyl chains, there is penetration of between 50 and 60% of the total number of counter ion methyl groups into the fluorocarbon region of the lamellar phase. These bound counter ions reduce the accessibility of the head group region to solvent water. As the number of butyl chains on the counter ion increases the lamellar phase is progressively lost and is replaced by a reversed micelle phase either as a single phase or as part of an extensive two phase region.

## Introduction

Fluorocarbon surfactants have rigid hydrophobic chains and high hydrophobic volumes compared with their hydrocarbon homologs.[1–5] This influences the molecular shape and in turn, their aggregate geometry.[6,7] Fluorocarbon surfactants tend to form layered aggregate structures, such as lamellar[8] and mesh phases.[9–16] A random mesh phase, $Mh_1(0)$ was found in the cesium perfluorooctanoate (CsPFO)/water system.[10–15] The random mesh phase is a lamellar phase where the bilayers are pierced by water filled holes and was first reported as perforated vesicles by Hoffmann *et al.*[17] A correlated mesh phase, $Mh_1(I4m)$ with tetragonal symmetry was found in the lithium perflurooctanoate (LiPFO)/water system,[16] and in the tetramethylammonium perfluorodecanoate ($C_{10}$TMA)/water system,[10] a correlated mesh phase, $Mh_1(R\bar{3}m)$ with rhombohedral symmetry was observed.

The $Mh_1(R\bar{3}m)$ phase in the $C_{10}$TMA/water system is extremely stable to both temperature and concentration. It has a layered structure similar to that of the $Mh_1(0)$ phase, but the water filled defects are correlated between layers. The water filled defects are holes which are arranged in a hexagonal structure, with the holes in one layer positioned over the nodes in the layers below in an ABCA stacking, Fig. 1. The space group and structure for the phase is similar to that of equivalent phases found in $C_{16}EO_6$/water,[18–20] $C_{30}EO_9$/water systems,[21] $TA_{16}SO_7$/water,[22] and CTAB/SHN/water[23,24] which demonstrates that a 3-connected mesh layer structure is the preferred structure.[18,19] In this structure, the surfactant mesh layer is continuous, and possesses a constant mean curvature to reduce the elastic bending energy.[18,23–25]

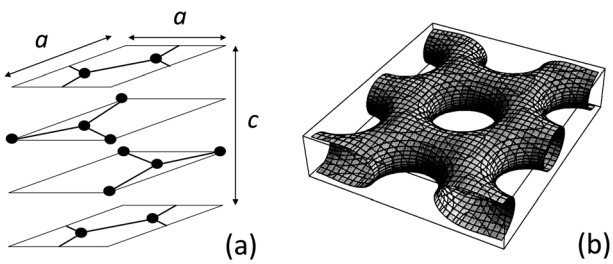


**Fig. 1** (a) A schematic illustration of the rhombohedral unit cell of the $Mh_1(R\bar{3}m)$ phase showing the location of the mesh nodes and the interconnecting rods. (b) A mean curvature model of a single mesh layer.[1]

[a]*School of Forensic and Investigation Science, University of Central Lancashire, Preston, PR1 2HE, UK*
[b]*Graduate Research School, University of Central Lancashire, Preston, PR1 2HE, UK*
[c]*Unilever Research and Development Port Sunlight, Quarry Road East, Wirral, CH63 3JW, UK*
[d]*St Mary's Catholic College, St Walburga's Road, Blackpool, FY3 7EQ, UK*

The structural parameter $c/a$, defined in Fig. 1, for $Mh_1(R\bar{3}m)$ in the C10TMA system is in the range from 2.0 to 2.4; a similar range of $c/a$ is observed in $C_{16}EO_6$/water[18–20] and $C_{30}EO_9$/water systems.[21] The reason for the $Mh_1(R\bar{3}m)$ phase forming in the $C_{10}$TMA/water system is not clear. It is possible that the hydrophobic counter ion TMA facilitates formation of the structure.

Previous studies on the salts of perfluorononanoic acid in dilute solution showed that when ammonium counter ions are partially substituted by alkyl groups there was evidence for giant micelles with the surfactant ions and counter ions solubilised as ion pairs inside the micelles.[26] In the recent work of Klaus *et al.*[27] on the salting in and salting out effects of counter ions on the large surfactant, X-AES in aqueous solution, the addition of the hydrotrope, sodium xylene sulfonate causes the latter to be pushed into the hydrophobic core of the micelles by adding divalent ions.

For the $C_{10}$TMA/water system, when the counter ion, TMA was replaced by tetrabutylammonium (TBA)[8] the surfactant system displayed a unique phase behaviour that had an extensive reversed micellar phase, $L_2$ over a wide region of concentration. Between the normal micelle phase, $L_1$ and the $L_2$ phase, a lamellar phase, $L_\alpha$ and two phase regions were observed. X-ray scattering experiments confirmed that the lamellar phase consisted of a classical bilayer structure with no defects; however, the bilayer thickness was calculated to be much less than the fully extended fluorocarbon chain.[8] When the bilayer thickness was recalculated including 2–3 butyl chains per counter ion into the bilayer volume, more realistic values were obtained. There is evidence of the hydrophobic counter ions are being partially solubilised in the hydrophobic core.

Both tetramethylammonium and tetrabutylammonium are hydrotropic which by themselves are unable to form micelles and facilitate anisotropic phases.[28] However, the addition of hydrotropic counter ions to surfactant systems with the same hydrophobic $C_{10}$ chains causes different phase behaviour. Counter ions with hydrophobicities between TMA and TBA provide an opportunity to study the causes of the phase behaviours.

The molecular packing parameter[7] $v/a_o l_C$ is thought to be key to describing the micellar shape and the mesophase structure. $v$ is the volume of the hydrophobic chain and $l_C$ is the critical hydrophobic chain length, which sets a limit on how far the hydrophobic chain can extend and is generally less than the maximum *all-trans* chain length.[29,30] $a_o$ is the optimal surface area per molecule at the water-fluorocarbon interface. It has been shown that the value of $v/a_o l_C$ is related to the aggregate shape so that for spherical micelles $v/a_o l_C < 1/3$, for non-spherical micelles $1/3 < v/a_o l_C < 1/2$, for bilayers or layered structures $1/2 < v/a_o l_C < 1$ and for inverted structures $v/a_o l_C > 1$. Cryo-TEM experiments were carried out on dilute perfluorodecanoate surfactant and water systems,[31] with counterions ammonium (A), tetramethylammonium (TMA), butyltrimethylammonium (BTMA), dibutyldimethylammonium (DBDMA), and tetrabutylammonium (TBA). The aggregate is changed from sphere, rod to vesicle and bilayer, which is reflected in an increased in $v/a_o l_C$. It is thought this is caused by a reduction in the surface area per molecule and is driven by increased counter ion binding to the surface of the aggregate as the hydrophobicity of the counter ion increases.

Here we report hydrophobic counter ion effects on the concentrated phases of a series of perflurodecanoate (C10) surfactants with counter ions of increasing hydrophobicity; tetramethylammonium (TMA), butyltrimethylammonium (BTMA), dibutyldimethylammonium (DBDMA), and methyltributylphosphonium (MTBP). They were studied using small angle X-ray scattering (SAXS), and $^2$H NMR. The C10 surfactant with methyltributylammonium (C10MTBA) could not be synthesised with sufficient purity, and was replaced by C10MTBP.

## Experimental

### Synthesis of fluorocarbon surfactants

The series of fluorocarbon surfactants were made by neutralisation of the perfluorodecanoic acid with the hydroxide of the related hydrophobic counter ions, *i.e.* tetramethylammonium hydroxide (TMAOH), butyltrimethylammonium hydroxide (BTMAOH), dibutyldimethylammonium hydroxide (DBDMAOH) and methyltributylphosphonium hydroxide (MTBPOH). MTBPOH was synthesised using the following procedure:

### Synthesis of tributylmethylphosphonium iodide

Under an inert atmosphere of nitrogen tributylphosphine (0.05 moles, 10.13 g) was added to distilled toluene (20 ml) and cooled in an ice bath. Iodomethane (0.05 moles, 7.11 g) was added and the solution heated under reflux, with stirring, for 24 h, the solution becoming yellow in colour. On cooling to room temperature white crystals appeared. The crystals were removed by filtration under vacuum and dried in air. Recrystallisation from a mixture of ethyl acetate and diethyl ether (ratio 1 : 1) produced the title compound as a white crystalline solid (16.1 g, 94%); m.p. 132–134 °C (lit.[32] 131–132 °C); $C_{13}H_{30}IP$ requires C 45.36%, H 8.78%, found C 45.36%, H 8.80%; δ $^{31}$P ($CDCl_3$, 101.2MHz) ppm 32.43; δ $^1$H ($CDCl_3$, 250.1MHz) ppm 0.91 (9H, t, $J$ 6.8, $CH_2C\underline{H}_3$), 1.46-1.55 (12H, m, $CH_2(C\underline{H}_2)_2CH_3$), 2.03 (3H, d, $J$ 13.31, P–$CH_3$), 2.40 (6H, dt, $J_{P\text{-}H}$ 13.21, $J_{H\text{-}H}$ 6.8, P-$C\underline{H}_2CH_2$).

### Synthesis of tributylmethylphosphonium nonadecaflurodecanoate

Tributylmethylphosphonium iodide (5.8 mmoles, 2 g) was dissolved in absolute ethanol (30 ml) and cooled in ice. Ion-exchange resin (Amberlite IRA-420 (OH)) (15 g) was added and the solution stirred for 1.5 h until testing with silver nitrate indicated no halide remained in solution. The resin was removed by filtration under vacuum. The filtrate was kept in ice to prevent conversion to a phosphine oxide. A small portion of the filtrate was titrated with nonadecafluorodecanoic acid (7.78 mmoles, 4 g) in a mixture of ethanol and water (ratio 1 : 1) and the pH recorded over the addition. A graph was plotted to determine the endpoint of the reaction, which occurred at a pH of 6.6. The solution was taken back to a pH of 6.6 with a further small portion of the filtrate, producing a thick pale yellow solution.

The remainder of the tributylmethylphosphonium iodide (0.04 moles, 14 g) was dissolved in absolute ethanol (150ml) and cooled in an ice bath. Ion-exchange resin (60 g) was added and

 

the solution stirred for 3 h in an ice bath to keep the solution cool. Testing with silver nitrate showed no halide remained. The resin was removed by filtration under vacuum and the filtrate reacted with nonadecafluorodecanoic acid (0.04 moles, 20.9 g) giving a pH of 6.6. The solvent was removed under vacuum producing an orange oil. The oil was heated to 60 °C and on cooling under vacuum pale yellow crystals were produced. Drying under vacuum for several days produced the title compound as pale yellow hygroscopic crystals, requiring storage under argon. (34.19 g, 100%); m.p. 39 °C; $C_{23}H_{30}F_{19}O_2P$ requires C 37.82%, H 4.14% found C 37.81%, H 4.31%; ν (Nujol) $cm^{-1}$: 1693 (C═O), 1240 (s), 1217 (C–F), 1151 (s); δ $^{31}P$ ($CDCl_3$, 101.2MHz) ppm 33.42; δ $^{1}H$ ($CDCl_3$, 250.1MHz) ppm 0.98 (9H, t, $J$ 6.8, $CH_2C\underline{H}_3$), 1.48–1.57 (12H, m, $CH_2(C\underline{H}_2)_2CH_3$), 2.02 (3H, d, $J_{P\text{-}H}$ 13.55, P-$CH_3$), 2.33 (6H, dt, $J_{P\text{-}H}$ 13.28, $J_{H\text{-}H}$ 6.8, P–$C\underline{H}_2CH_2$).

BTMAOH and DBDMAOH were obtained in a similar manner to MTBPOH by reacting butyldimethylamine with either iodomethane or 1-bromobutane to form the quaternary ammonium salts, followed by reaction with the strong base form of Amberlite IRA 420 (OH) to exchange the halide ion for hydroxide ion in aqueous solutions. The highly alkaline solutions were neutralised with stoichiometric amounts of the perfluorodecanoic acid and the pH of each solution was checked for neutrality (pH 6.6) using a pH electrode. The water solvent was removed *in vacuo* at 40–45 °C to give a pale solid. The purity of each compound involved in the synthesis of the surfactants was confirmed by elemental analysis and $^{1}$H-NMR spectroscopy.

### Preparation of samples

The surfactant samples were prepared using $^{2}H_2O$ (Fluka, purity >99.8%). The required amount of surfactant and $^{2}H_2O$ were weighed out into a sample tube containing a constriction (to aid mixing) and then flame sealed. Sample homogenisation was achieved by vortex mixing, repeated centrifuging, or oven heating to 60 °C (if no phase separation occurred) and was checked by viewing by the naked eye and between crossed polarisers. These samples were equilibrated at room temperature. 5mm NMR tubes (from Fluorochem Ltd.), and 0.7mm or 0.5mm Lindeman capillaries tubes (from Pawtak Ltd.) were also prepared by transferring from the bulk sample tube and flame sealing the open ends.

## Characterisation methods

### $^{2}$H NMR

A Bruker Advance DPX250 NMR spectrometer was used, operating at 38.3MHz for deuterium nuclei. Samples were equilibrated at a temperature with an accuracy of ±0.1 °C for 30 min prior to recording spectra. The temperature dependence of the quadrapolar splitting of $^{2}H_2O$ was recorded on heating or cooling depending on how the sample changed from one-phase to two-phase regions.

### Small Angle X-ray Scattering (SAXS)

SAXS experiments were conducted both in Preston and at the Synchrotron Radiation Source, Daresbury Laboratories in Warrington. At the University, Cu-Kα X-rays with a wave length of 0.154 nm were produced using a Philips PW1830 X-ray generator operating at 45 kV and 25mA and a Philips fine focus tube. The 0.5mm Lindeman capillary tubes were held in a copper block, and the temperature was controlled by a Haake F3 heater and DK 12 pump flow, with an accuracy of ±0.1 °C. The scattered radiation was detected by a Photonics Science CCD detector, and the data was analyzed using the DIS 3000 imaging suite.

At the Daresbury Laboratories, SAXS experiments were carried out at Station 2.1. The X-ray wavelength was 0.154 nm, and a camera length of 1.50 m was used, with exposure times between 3 and 5 min. The samples in 0.7 mm Lindmann capillary tubes were held in a Linkham THM600 sample stage with the temperature controlled by a Linkham TMS91 unit (accuracy ±0.1 °C). The scattering data was processed using BSL and XOTOKO programs.

## Results and discussion

### The phase diagrams

Fig. 2 represents the surfactant and water binary phase behaviours of the perfluorodecanate salts with counter ions TMA, BTMA, DBDMA, and MTBP, at 25 °C. For C10MTBP, the lamellar phase is not extensive at 25 °C, and therefore the phase behaviour at 10 °C is also shown in order to provide a larger lamellar region for measurement. The phases were determined by using samples with a range of surfactant concentrations which were studied on heating and cooling through the temperature in question. The detailed phase diagrams have been reported previously.[10,31]

Fig. 2 shows that there is a clear trend, C10TMA exhibits a sequence of mesh phases; both random and correlated over a wide range of concentrations from 13% to 87% by weight C10TMA. The substitution of a single methyl group on the counter ion by a butyl chain switches off all the mesh phases and replaces them with the lamellar phase over nearly the same concentration range. Replacement of further methyl groups by butyl groups causes the development of a reverse micellar phase, $L_2$ at high surfactant concentrations and with it a large two phase region between lamellar and $L_2$ phases. In C10MTBP this two phase region has expanded to occupy most of the middle of the phase diagram (20% to 70% by weight MTBP).

### X-ray scattering

Fig. 3 shows the bilayers spacing, $d_{\|}$ as a function of surfactant mole fraction. The observation of only two reflections with a ratio of 1 : 2 confirms a normal lamellar phase for all samples but C10TMA, where the observation of seven or eight reflections[18–20] confirms a highly ordered $Mh_1(R\bar{3}m)$ phase.

Care must be taken with the analysis of these results because unlike many surfactants with hydrophilic counter ions, these have large hydrophobic counter ions which constitute a significant proportion of the total sample volume. Also, since they are hydrophobic it is to be expected that a significant proportion of the counter ions will be associated with the hydrophobic bilayers. This will have the effect of increasing the hydrophobic volume

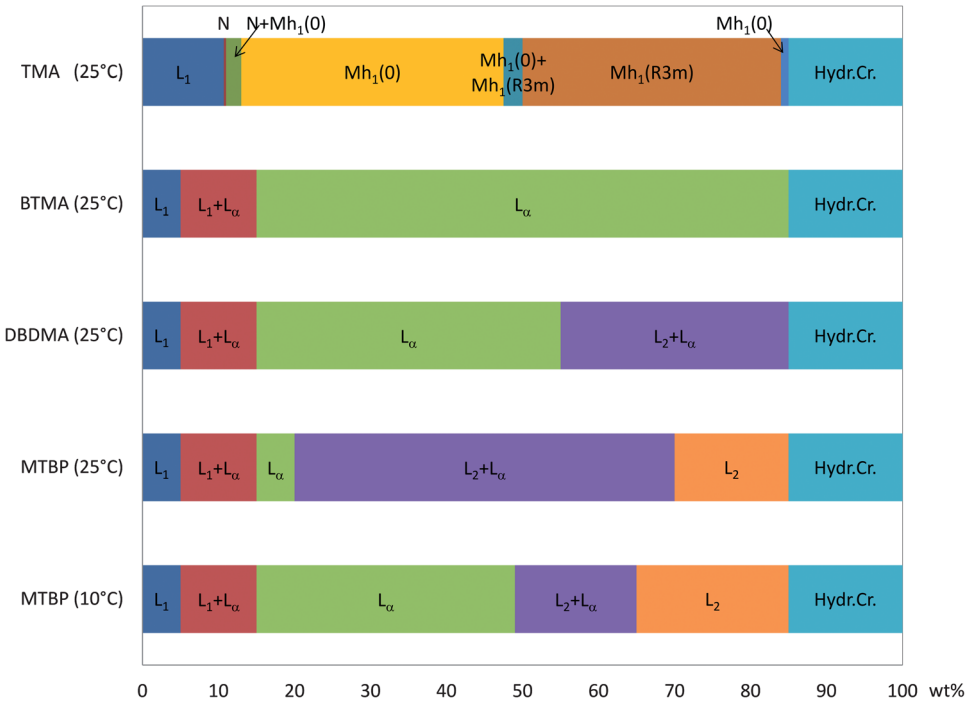


**Fig. 2** Isothermal surfactant and water binary phase diagrams of perfluorodecanoic salt with counter ions TMA, BTMA, and DBDMA at 25 °C, and MTBP at both 25 °C and 10 °C. The phases observed are as follow: $L_1$, isotropic micellar phase; N, nematic phase; $Mh_1(0)$, random mesh phase; $Mh_1(R\bar{3}m)$, correlated mesh phase; $L_\alpha$, lamellar phase; and Hydr.Cr., hydrated crystals.

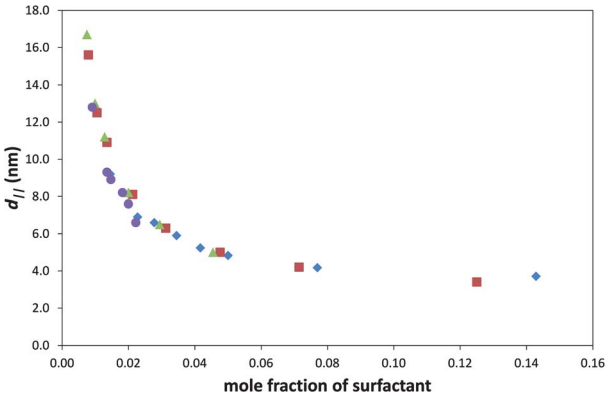


**Fig. 3** The bilayer spacing, $d_\parallel$ as a function of surfactant mole fraction measured by X-ray scattering for C10TMA (◆), C10BTMA (■) and C10DBDMA at 25 °C (▲) and C10MTBP at 10 °C (●).

fraction, $\varphi_{hydrophobic} \approx \varphi_{surf}$, where the latter is the volume fraction of the whole surfactant including the counter ion and is given by.

$$\varphi_{surf} = \frac{V_{fc} + V_{COO} + V_{ion}}{V_{fc} + V_{COO} + V_{ion} + NV_{D2O}} \quad (1)$$

where the molecular volumes are: $V_{fc}$, fluorocarbon chain; $V_{COO}$, carboxyl head group; $V_{ion}$, counter ion; $V_{D2O}$, deuterium oxide and $N$ is the water surfactant mole ratio. Generally, for all the studied surfactants, as the water content increases, the bilayer separation, $d_\parallel$ increases. If the phase is a classical bilayer without any water filled defects the bilayer thickness can be calculated from

$$d^*_{hydrophobic} = d_\parallel \varphi_{surf} \quad (2)$$

where $d^*_{hydrophobic}$ is the apparent thickness of the hydrophobic bilayers including the counter ions. However, in the case of C10TMA, X-ray scattering shows the presence of mesh phases containing water filled holes. For any surfactant phase structure, eqn (2) takes the more general form

$$d^*_{hydrophobic} = d_\parallel \varphi_{surf}{}^x \quad (3)$$

where $x = 1$ for a perfect lamellar phase, $x = 0.5$ for a hexagonal phase and $x = 0.33$ for a micelle or cubic phase. A mesh phase will have $1 > x > 0.5$.

Fig. 4 shows the power law fits to the experimental data with the fit parameters summarised in Table 1.

The values of $x$ confirm the lamellar phase identifications in C10BTMA, C10DBDMA, and C10MTBP. For C10TMA, $x = 0.79$ which is consistent with a mesh phase. For C10TMA,

$$d^*_{hydrophobic} = 2.89 \text{ nm}$$

at zero water content. This system has the smallest amount of hydrocarbon in the counterion and therefore the minimum inter penetration of hydrocarbon into the fluorocarbon bilayer. The normal fluorocarbon bilayer thickness $d_{fc}$ can be calculated from:

$$d_{fc} = d^*_{hydrophobic}\left(\frac{V_{fc}}{V_{fc} + V_{coo} + V_{ion}}\right)$$

which gives $d_{fc} = (1.93 \pm 0.05)$ nm at zero water content. This value can be used to calculate the water content of the water filled pores in the mesh phases.

 

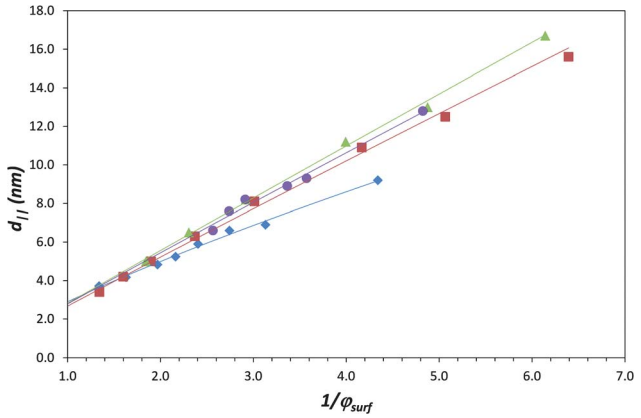


**Fig. 4** The bilayer spacing as a function of $1/\varphi_{surf}$. Symbols are defined in Fig. 3. The curves are power law fits using eqn (3).

**Table 1** Results from the power law fits, eqn (3), to the data in Fig. 4

| Surfactant | $x$ (±0.01) | Coefficient of Determination, $R^2$ | $d^*_{hydrophobic}$ (±0.05) nm |
|---|---|---|---|
| C10TMA | 0.79 | 0.994 | 2.89 |
| C10BTMA | 0.97 | 0.997 | 2.67 |
| C10DBDMA | 0.98 | 0.998 | 2.82 |
| C10MTBP (at 10 °C) | 0.97 | 0.966 | 2.79 |

### Calculating the water content of the mesh layers in C10TMA

For the C10TMA system an estimate of the volume fraction of the mesh layers made up of water filled holes, $f$ can be obtained using a different form of eqn (2):

$$d^*_{hydrophobic} = \frac{d_{||}\varphi_{surf}}{(1-f)}$$

Whilst Fig. 5 demonstrates that the volume fraction of water in the mesh layers decreases with decreasing water content, the absolute values of $f$ depend upon the number of TMA ion methyl groups contributing to the mesh layer volume fraction, $\varphi_{surf}$.

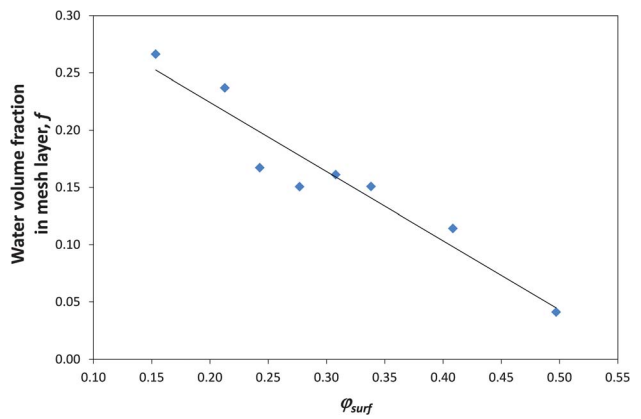


**Fig. 5** The volume faction of water in the mesh layer $f$ (solid line) calculated from eqn (3) with $d^*_{hydrophobic} = 2.89$ nm and assuming the counter ions are included within the hydrophobic region.

### Calculating the hydrocarbon content of the lamellar bilayers

It is also interesting that in all four systems the curves in Fig. 4 extrapolate back to a bilayer separation of about 2.8 ± 0.1 nm at zero water content corresponding to twice the all-*trans* $C_{10}$ chain length.

The thickness of the fluorocarbon bilayer, $d_{fc}$ is unlikely to change significantly because of the rigidity of the fluorocarbon chains. The hydrophobic counter ions occupy spaces of similar dimensions between the water and fluorocarbon layer because of the hydrocarbon chain folding and interdigitation between the fluorocarbon chains of the bilayer. As the number of butyl chains on the counter ion increases so too does the interpenetration of butyl chains into the bilayer. This is represented schematically in Fig. 6.

Fig. 4 and Table 1 show that the three systems C10BTMA, C10DBDMA, and C10MTBP behave differently to C10TMA with $x$ being nearly unity (Table 1), demonstrating ideal lamellar phase swelling behaviour. If it is assumed that there is no inter penetration of hydrocarbon groups from the counter ions into the fluorocarbon bilayer, apparent bilayer thickness, $d^*_{fc}$ can be calculated from

$$d^*_{fc} = d_{||}\varphi_a$$
$$\text{where } \varphi_a = \frac{V_{fc}}{V_{fc} + V_{COO} + V_{ion} + NV_{D2O}} \quad (4)$$

Within each system $d^*_{fc}$ is roughly constant with changing $\varphi_a$, see Fig. 7. However $d^*_{fc}$ decreases as the number of butyl chains increase. This implies that butyl chains and methyl groups from the counter ions are being bound into the hydrophobic bilayer, increasing its volume fraction, $\varphi_a$.

Clearly some of the hydrocarbon groups are entering the fluorocarbon bilayer. This can be estimated by modifying eqn (4) to include the volume associated with hydrocarbon chains in the fluorocarbon bilayer,

$$\varphi_a = \frac{(V_{fc} + nV_{CH})}{(V_{COO} + V_{FC} + V_{ion} + NV_{D2O})} \quad (5)$$

where $n$ is the number of $CH_2$ or $CH_3$ groups of volume $V_{CH}$ in the bilayer.

Rearranging eqn (5) gives:

$$n = \frac{\varphi_a(V_{COO} + V_{fc} + V_{ion} + NV_{D2O}) - V_{fc}}{V_{CH}}$$

The volume fraction, $\varphi_a$ is now replaced by $d_{fc}/d_{||}$, where $d_{fc} =$ 1.93 nm. The results for each system are approximately constant and are summarised in Table 2.

The results show that a significant proportion of the $CH_2$ and/or $CH_3$ groups on the counter ions are within the bilayer volume. In C10BTMA and C10DBDMA this is likely to be one butyl chain and in C10MTBP two butyl chains will be contributing to the bilayer volume. The surface area per surfactant molecule at the water/fluorocarbon interface, $s_a$ can be calculated from

$$s_a = 2\frac{(V_{fc} + nV_{CH})}{d_{fc}}$$

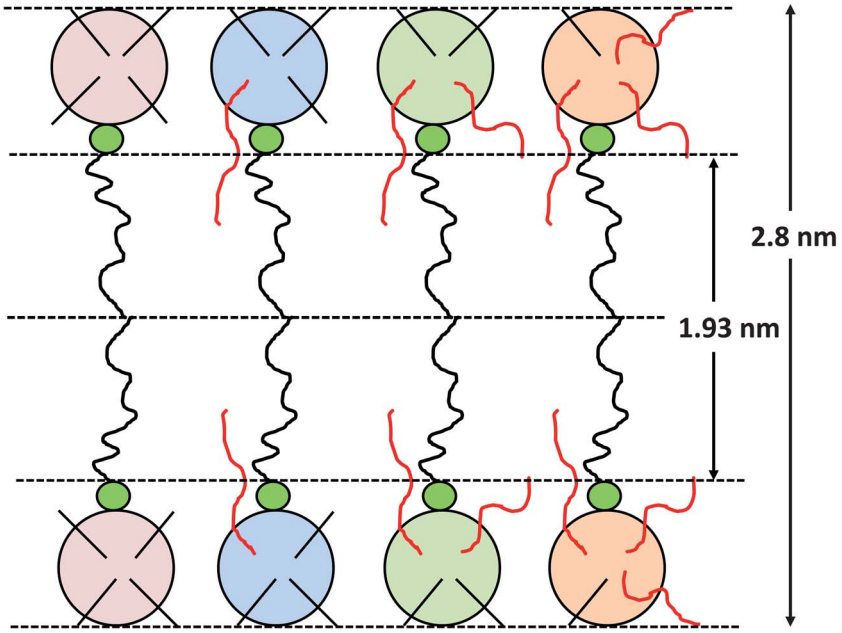


**Fig. 6** A schematic illustration of hydrophobic counter ion binding. The counter ions are represented as follows: TMA – pink, BTMA – blue, DBDMA – green and MTBP – orange. Butyl chains are represented by the red lines.

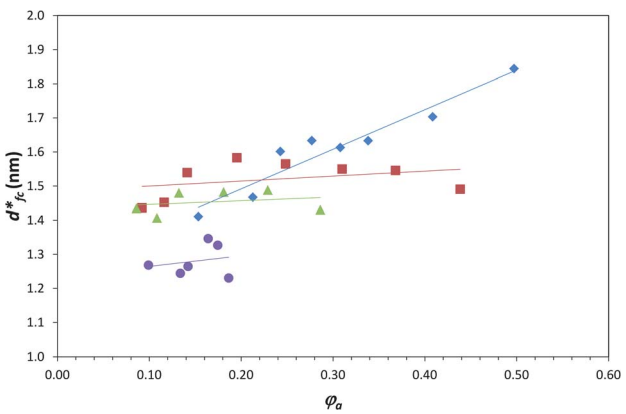


**Fig. 7** $d^*_{fc}$ as a function of $\varphi_a$. Solid lines are a guide to the eye. Note that $d^*_{fc}$ varies very little with $\varphi_a$ Symbols are defined in Fig. 3.

The results in Table 2 show that as the number of $CH_2$ or $CH_3$ groups associated with the bilayer increases, $s_a$ increases. A further insight into the binding of the hydrophobic counter ions can be obtained from the $^2H$ NMR spectrum of the solvent $^2H_2O$.

### $^2H$ NMR results

The evolution of the quadrapolar splitting, Δ with the mole ratio of surfactant to water, $X_s$ in phases with layered structures for C10 systems with different counter ions is illustrated in Fig. 8. For all the systems, Δ varies monotonically with mole ratio. The quadrapolar splitting, Δ is proportional to two factors in these systems. First it is dependent upon the fraction of water molecules bound to the interface and that is directly proportional to the mole ratio of surfactant and water. Second it depends upon the interfacial curvature of the surfactant water interface. This can be expressed as:

$$\Delta = \Delta_o p S_c \quad (6)$$

where $\Delta_o$ is the fundamental quadrapolar splitting for each system. $p$ is the fraction of water bound to the surfactant water interface, and is proportional to $X_s$, *i.e.* $p = kX_s$ where $k$ is a constant. $S_c$ is an order parameter which expresses the

**Table 2** The number, $n$ of $CH_{2/3}$ groups contributing to the bilayer volume for C10BTMA, C10DBDMA and C10MTBP. Note that C10MTBP is at 10 °C where more counter ion binding might be expected

| Surfactant | n the number of CH2/3 groups associated with the bilayer volume per counter ion | Total number of CH2/3 groups on the counter ion | Percentage of CH2/3 groups on the counter ion associated with the bilayer volume | Surface area per surfactant molecule at the water/ fluorocarbon interface, $s_a$ (nm$^2$) |
|---|---|---|---|---|
| C10BTMA | 4.1 ± 0.7 | 7 | 59 ± 10 | 0.54 ± 0.02 |
| C10DBDMA | 5.0 ± 0.7 | 10 | 50 ± 7 | 0.57 ± 0.02 |
| C10MTBP (at 10 °C) | 7.8 ± 0.7 | 13 | 60 ± 6 | 0.65 ± 0.02 |

 

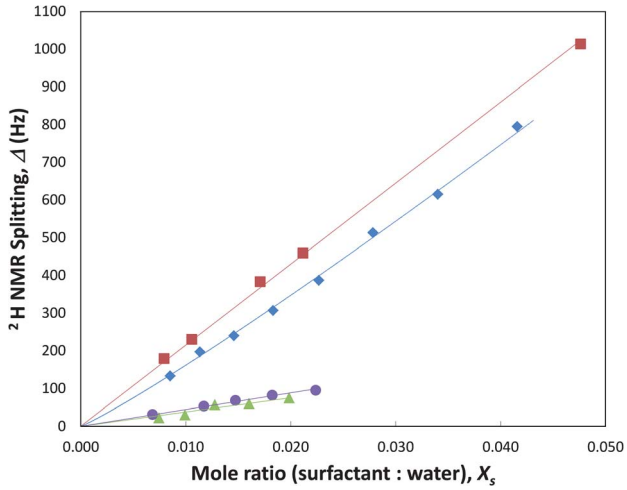


**Fig. 8** Variation of $^2$H NMR splitting *versus* mole ratio of surfactant to water, $X_s$ for C10TMA, C10BTMA and C10DBDMA at 25 °C and C10BTMP at 10 °C. The curves are linear fits except for C10TMA which is a power law fit of the form $\Delta = 26069\ X_s^{1.1}$. Symbols are defined in Fig. 3. All fits have coefficients of determination, $R^2$ better than 0.98.

curvature of the interface and varies between unity for a perfect lamellar phase and zero for a spherical micelle. $S_c$ has a more complex dependence upon $X_s$ which depends upon the geometry of the mesh phase aggregates.

The C10BTMA, C10DBDMA and C10MTBP systems are all lamellar phases and, therefore Fig. 8 shows that at a fixed value of $X_s$ $p_{C10BTMA} > p_{C10DBDMA} \cong p_{C10MTBP}$. As the counter ion becomes more hydrophobic and more $CH_2$ and $CH_3$ groups are bound into the fluorocarbon layer so it becomes more difficult for water to bind to the head group region and the fraction of bound water decreases; thus confirming the conclusions of the previous section.

Fig. 8 shows that the results for C10TMA do not fit with a linear dependence of Δ against $X_s$. A power law fit shows $\Delta = 26069 X_s^{1.1039}$. The departure from linearity is because both $p$ and $S_c$ are changing with $X_s$. Assuming that $\Delta_o k = 21.5$ kHz, the same as for the C10BTMA system, values of $S_c$ can be estimated for the C10TMA system from a modification of eqn (6)

$$S_c(X_s) = \frac{\Delta}{\Delta_o k X_s} \tag{7}$$

Fig. 9 shows $S_c$ calculated from eqn (7) for C10TMA as a function of $X_s$. Whilst the values of $S_c$ are reasonable and consistent with the values of $f$ obtained in the previous section, they should be regarded as estimates because of the assumptions made to obtain them. Unfortunately there is no clear relationship between $S_c$ and $f$ without further geometrical assumptions about pore size and structure. Fig. 9 illustrates that $S_c$ increases as the mesh holes diminish in size reducing the amount of interfacial curvature.

## Discussion

The hydrophobicity of the counter ion has a profound effect upon the phases formed in these perfluorodecanoate/water systems. Fig. 2 shows that it is only with the TMA counter ion

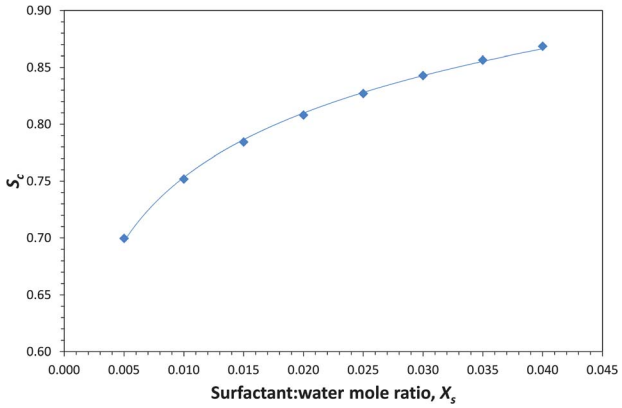


**Fig. 9** An estimate of the curvature order parameter, $S_c$ as a function of $X_s$ calculated from eqn (7). The curve is a guide to the eye.

that mesh phases are formed to the exclusion of all other phases including the lamellar phase. The replacement of one methyl group by a butyl group on the counter ion replaces the mesh phases by a lamellar phase and further substitution of methyl by butyl groups leads to the replacement of the lamellar phase by a reversed micellar phase, $L_2$. The cause of these phase changes is the association of the hydrophobic groups on the counter ion with the hydrophobic region of the bilayer. The TMA counter ion has sufficient of its methyl groups within the head group region to allow the interface to form the curved interface associated with a mesh phase. This phase may be either a random mesh or a rhombohedral mesh. At the local, mesh layer level these two phases have very similar structures; their differences lie in the degree of correlation between layers. This is controlled to some degree by the concentration of counter ions.

The substitution of a single methyl group in the TMA counterion by a butyl chain causes the replacement of all mesh phases by the lamellar phase, and it is apparent from Table 2 that this single chain is closely associated with the hydrophobic fluorocarbon core. Increasing the number of butyl chains to two does, not increase the number of associated chains in the lamellar phase substantially, Table 2 but it does allow the formation of a stable $L_2$ phase to be formed at higher surfactant concentration. The negative interfacial curvature of the $L_2$ phase has a more favorable geometry for binding counter ions with more butyl chains.

The surfactant parameter can now be used to look at the effect of increasing the number of butyl chains on the counter ion. The surfactant parameter, $v/a_o l_C$ can be calculated by putting $a_o = s_a$, $l_C = d_{fc}/2$ and $v = v_{fc} + v_{COO} + qV_{butyl}$ where $V_{butyl}$ is the volume of a butyl chain and $q$ is the number of butyl chains associated with a fluorocarbon core. Table 3 shows the results of calculating $v/a_o l_C$ for each surfactant system.

The surfactant parameter for C10BTMA is unity and consistent with the formation of an $L_\alpha$ phase and no reversed, $L_2$ phase. As the number of butyl chains increase the surfactant parameter calculated for all available chains being associated with the fluorocarbon region increases above unity demonstrating that the $L_2$ phase becomes increasingly more favourable than the $L_\alpha$ phase.

**Table 3** The surfactant parameter, $v/a_o l_C$ calculated for C10BTMA, C10DBDMA and C10MTBP. Symbols are defined in the text

| | $q$ | $a_o$ (±0.02) nm$^2$ | $l_C$ (±0.03) nm | $V$nm$^3$ | $v/a_o l_C$ (±0.04) |
|---|---|---|---|---|---|
| C10BTMA (25 °C) | 1 | 0.54 | 0.97 | 0.521 | 1.00 |
| C10DBDMA (25 °C) | 2 | 0.57 | 0.97 | 0.629 | 1.14 |
| C10MTBP (10 °C) | 3 | 0.65 | 0.97 | 0.737 | 1.21 |

## Conclusions

The study has verified the mesh phase structure in the C10TMA system independently of the X-ray scattering pattern indexation.[10] It has also shown that the thickness of the hydrophobic layer at zero water content is approximately 2.8 nm for all the counter ion types and that it is possible to estimate the water fraction in the mesh phase using some simple physical assumptions. Using geometrical constraints it has been shown that typically 50 to 60% of hydrocarbon chains on any of the counter ions are associated with the hydrophobic regions of the lamellar phase and confirms the solubilisation of both the surfactant ions and counter ions postulated by Hoffmann *et al.*[26] $^2$H NMR spectra are consistent with these results, because the counter ion binding reduces the water binding and thereby the NMR splittings.

The hydrophobicity of the counter ion plays an important role in determining the phase structure of these perfluorocarbon surfactants in aqueous solution. In the case of C10TMA the counter ion serves to stabilise mesh phases (either correlated or not) across the range of surfactant concentrations from 15 to 85 weight percent surfactant. Substituting one methyl group by a butyl group causes this extensive mesh phase to be replaced entirely by a lamellar phase. Further substitution by butyl groups leads to the replacement of the lamellar phase by a reversed micellar phase. Key to this process is the incorporation of some of the hydrocarbon groups on the hydrophobic counter ions into the fluorocarbon bilayers. Formation of the reversed phase facilitates a more efficient incorporation because of the interfacial geometry.



## Acknowledgements

We would like to thank the University of Central Lancashire for the research funding for this project. RZ thanks Dr John Burgoyne for his help with the NMR experiments and Dr Anthony Gleeson in Station 2.1, Daresbury, for his help with SAXS experiments.

## References

1 M. C. Holmes, *Curr. Opin. Colloid Interface S.*, 1998, **3**, 485–492.
2 K. Fontell and B. Lindman, *J. Phys. Chem.*, 1983, **87**, 3289–3297.
3 E. Kissa, *Fluorinated Surfactants and Repellents*, Marcel Dekker Inc., New York, 2nd edn, 2001.
4 M. Monduzzi, *Curr. Opin. Colloid Interface S.*, 1998, **3**, 467–477.
5 K. Wang, G. Karlsson, M. Almgren and T. Asakawa, *Journal of Physical Chemistry B*, 1999, **103**, 9237–9246.
6 W. M. Gelbart, A. Ben-Shaul, and D. Roux, *Micelles, Membranes, Microemulsions, and Monolayers*, Springer-Verlag Inc., New York, 1994.
7 J. Israelachvili, D. J. Mitchell and B. W. Ninham, *J. Chem. Soc., Faraday Trans. 2*, 1976, **72**, 1525–1568.
8 A. M. Smith, M. C. Holmes, A. Pitt, W. Harrison and G. J. T. Tiddy, *Langmuir*, 1995, **11**, 4202–4204.
9 S. K. Ghosh and V. A. Raghunathan, *Langmuir*, 2009, **25**, 2622–2628.
10 S. Puntambekar, M. C. Holmes and M. S. Leaver, *Liq. Cryst.*, 2000, **27**, 743–747.
11 M. C. Holmes, M. S. Leaver and A. M. Smith, *Langmuir*, 1995, **11**, 356–365.
12 M. S. Leaver and M. C. Holmes, *J. De Phys. II*, 1993, **3**, 105–120.
13 M. C. Holmes, P. Sotta, Y. Hendrikx and B. Deloche, *J. De Phys. II*, 1993, **3**, 1735–1746.
14 M. C. Holmes, A. M. Smith and M. S. Leaver, *J. De Phys. II*, 1993, **3**, 1357–1370.
15 M. C. Holmes, A. M. Smith and M. S. Leaver, *J. De Phys. IV*, 1993, **3**(C8), 177–180.
16 P. Kékicheff and G. J. T. Tiddy, *J. Phys. Chem.*, 1989, **93**, 2520–2526.
17 H. Hoffmann, C. Thunig, U. Munkert, H. W. Meyer and W. Richter, *Langmuir*, 1992, **8**, 2629–2638.
18 M. S. Leaver, A. Fogden, M. C. Holmes and C. E. Fairhurst, *Langmuir*, 2001, **17**, 35–46.
19 C. E. Fairhurst, M. C. Holmes and M. S. Leaver, *Langmuir*, 1997, **13**, 4964–4975.
20 S. S. Funari and G. Rapp, *P. N. A. S.*, 1999, **96**, 7756–7759.
21 J. Burgoyne, M. C. Holmes and G. J. T. Tiddy, *J. Phys. Chem.*, 1995, **99**, 6054–6063.
22 B. F. B. Silva, E. F. Marques and U. Olsson, *Soft Matter*, 2011, **7**, 225–236.
23 S. K. Ghosh, R. Ganapathy, R. Krishnaswamy, J. Bellare, V. A. Raghunathan and A. K. Sood, *Langmuir*, 2007, **23**, 3606–3614.
24 R. Krishnaswamy, S. K. Ghosh, S. Lakshmanan, V. A. Raghunathan and A. K. Sood, *Langmuir*, 2005, **21**, 10439–10443.
25 S. T. Hyde and G. E. Schroder, *Current Opinion in Colloid & Interface Science*, 2003, **8**, 5–14.
26 H. Hoffmann, G. Platz, H. Rehage, K. Reizlein and W. Ulbricht, *Makromolekulare Chemie*, 1981, **182**, 451–481.
27 A. Klaus, G. J. Tiddy, R. Reinhard, A. P. Trinh, W. Maurer, D. Touraud and W. Kunz, *Langmuir*, 2011, **27**, 4403–4411.
28 S. E. Friberg, S. B. Rananavare and D. W. Osborne, *J. Colloid Interface Sci.*, 1986, **109**, 487–492.
29 N. Denham, M. C. Holmes and A. Zvelindovsky, *Journal of Physical Chemistry B*, 2011, **115**, 1385–1393.
30 J. F. Nagle and S. Tristramnagle, *Current Opinion in Structural Biology*, 2000, **10**, 474–480.
31 O. Regev, M. S. Leaver, R. Zhou and S. Puntambekar, *Langmuir*, 2001, **17**, 5141–5149.
32 W. A. Henderson and S. A. Buckler, *J. Am. Chem. Soc.*, 1960, **82**, 5794–5800.

 